C Journal of Carbon Research

MDPI

Article

Role of Graphene Oxide in Disentangling Amyloid Beta Fibrils

Brianna Duswalt [1], Isabella Wolson [2] and Isaac Macwan [1,*]

[1] Department of Electrical and Biomedical Engineering, Fairfield University, Fairfield, CT 06824, USA; brianna.duswalt@student.fairfield.edu
[2] Davidson School of Chemical Engineering, Purdue University, West Lafayette, IN 47907, USA; iwolson@purdue.edu
* Correspondence: imacwan@fairfield.edu; Tel.: +1-203-254-4000

Abstract: Recently, the accumulation of Amyloid Beta (Aβ) in the brain has been linked to the development of Alzheimer's disease (AD) through the formation of aggregated plaques and neurofibrillary tangles (NFTs). Although carbon nanoparticles were previously shown as having a potential to address AD, the interactions of Aβ with such nanoparticles have not been studied extensively. In this work, molecular dynamic simulations are utilized to simulate the interactions between a single atomic layer of graphene oxide (GO) and a 12-monomer Aβ fibril. These interactions are further compared to those between GO and five individual monomers of Aβ to further understand the conformational changes in Aβ as an individual monomer and as a component of the Aβ fibril. It was found that out of the 42 residues of the Aβ monomers, residues 27–42 are the most affected by the presence of GO. Furthermore, stability analysis through RMSD, conformational energies and salt bridges, along with nonbonding energy, illustrate that Aβ–Aβ interactions were successfully interrupted and dismantled by GO. Overall, the differences in the interactions between monomeric Aβ consisting of five monomers with GO, an Aβ fibril with GO, and control Aβ monomers among themselves, helped elucidate the potential that GO has to disentangle the Aβ tangles, both in case of individual monomers forming a cluster and as part of the Aβ fibril.

Keywords: amyloid beta; graphene oxide; molecular dynamics; Alzheimer's disease

Citation: Duswalt, B.; Wolson, I.; Macwan, I. Role of Graphene Oxide in Disentangling Amyloid Beta Fibrils. *C* **2024**, *10*, 88. https://doi.org/10.3390/c10040088

Academic Editor: Giuseppe Cirillo

Received: 12 August 2024
Revised: 20 September 2024
Accepted: 1 October 2024
Published: 3 October 2024

1. Introduction

According to the Center for Disease Control (CDC), Alzheimer's disease (AD) is the most common type of dementia. According to one study, approximately 5.8 million Americans are living with AD, with this number projected to reach 14 million by the year 2060. With that being said, AD has been categorized as the 6th leading cause of death among US adults [1]. Currently, there is no cure for AD, despite the large efforts made to find one, which has fueled the need to focus on solving the cause of AD rather than its effects. Based on the current understanding, the cause of AD is the aggregation of Amyloid Beta (Aβ) monomers within the brain, specifically the neocortex of the brain [2]. Whereas the discovery of plaques as well as the presence of neuro-fibrillary tangles in the brain of persons with dementia was made by Oskar Fisher and Lois Alzheimer in the early twentieth century [3], the presence of the protein Aβ that make up the plaques was more recently found in the mid-1980s by Glenner, Masters, and Beyreuther [4,5].

Aβ has been characterized as an enhancer of memory and a modulator of mitochondrial function. Amyloid is formed by a larger protein called the Amyloid Precursor Pro-tein (APP). In the sequence of breakdowns, a toxic split can occur at Aβ-42, referring to an Aβ containing 42 amino acids. The APP plays a crucial role in neural growth and maturation, through proposed methods such as the specification of cell identity, regulating proliferation, and the formation of neural stem cells [6]. The APP is cleaved by one of the two main enzymes, Beta Secretase and Alpha Secretase. However, the selectivity of one secretase to the APP versus the other is still unknown. In a healthy brain, Alpha Secretase cleaves to

the APP into sAPPalpha which protects neurons, acts as a stabilizer, and enhances memory. Conversely, Beta Secretase cleaves the APP to create sAPPbeta, which prunes synapses during neuron development. The ultimate result of Beta Secretase selectivity is Aβ-42 or Aβ-40, referring to Aβ with either 42 or 40 amino acids [6,7]. This specific strand of Aβ is particularly unfavorable. Aβ 42/40 forms clusters with itself by starting as dimers, further leading to insoluble hard aggregates that reside between the nerve cells attaching to their ends and eroding the synapse. This erosion interrupts neuronal transfer of information and the neuron's ability to repair and metabolize [8,9]. Although the specific mechanism of folding is yet unknown, studies are being conducted to thoroughly map out the Aβ oligomer formation to target specific mechanism steps and shut down oligomerization before it happens [10]. Since that action is a premature method for hindering AD development, one possible solution to eliminating the Aβ aggregates is dissolution. Therefore, the effort of this study focuses on the effect of dissolving the formed oligomers as opposed to eliminating Aβ's ability to oligomerize.

Conversely, the APP was also cited for its involvement in memory formation through changes in signal transduction events. Overall, the APP has many roles and plays an important role in the cascade leading to memory development. However, an accumulation of Aβ, specifically the APP, was shown to decrease the function of Translocase of the Outer Mitochondria Membrane Homolog (TOMMO40). This in turn leads to a decrease in the trans-location of essential proteins for mitochondrial function [11]. Therefore, Aβ enhances memory in acceptable quantities, but it is harmful when there is an accumulation of it. The aggregation of amyloid beta has been characterized as being most ideal with a protofilament conformation of larger oligomers of up to 12 Aβ monomers. At a size of around 12 Aβ monomers, a growth mechanism forms fibrils from these monomers [12]. These monomers have been established as blocking the neurons in the brain from performing their essential functions [9,13]. This lack of ability to perform properly then causes the neurons to die, thereby increasing the number of dead neurons in the brain and causing the brain to shrink, also known as brain atrophy, which causes memory loss. These aggregates also cause poor sleep [14] as well as several other major functionality issues such as cerebrovascular disease and Lewy body disease [13]. It is important to note that neurofibrillary tau tangles were shown to contribute to the same neuron-hindering effects as Aβ; however, this work does not include studying such neurofibrillary tau tangles. This is due to the fact that the tau tangles manifest later in the development of AD, and this study intends to focus on the earlier contributor, Aβ [15].

To address these issues, researchers have been trying to develop ways to dissolve Aβ-42 to hinder its damaging abilities to the brain. In recent studies, graphene oxide (GO) was found to have versatile potential for future AD detection and treatment. Some of the uses of GO include both biosensor and nanofiltration applications [10,16]. As a biosensor, GO was implemented to monitor and detect monomer, oligomer, and fibril Aβ concentrations [2]. Furthermore, RGO (reduced form of graphene oxide) can be used as a biosensor substrate to detect amyloid buildup to diagnose neural diseases [16]. GO is also used to decrease the detected amyloid plaques [17]. In recent simulations and trials, the amyloid build-up has been delayed by methods such as laser irradiation with GO [18] or by adsorption of Aβ by GO [17] under standard conditions. The principle in such methods is that GO interferes with the fibrillation of Aβ (where fibrillation is the proteins misfolding to the undesirable beta sheets) and extracts the amyloid monomers [17]. Yet, further analysis at the molecular level into specific mechanisms by which GO interacts with Aβ are still just theoretical and remains yet to be investigated. However, GO has already shown positive results in the progression of misfolding Aβ aggregates in previous studies [19]. For this reason, GO is being widely researched owing to its multifunctional potential in having a large reactive surface area and electric properties. A GO surface area holds promise as an avenue to attract, attach, and conformationally disconnect Aβ from each other. It was recently studied as a biosensor and a dissolving agent, where it was implemented to monitor and detect monomer, oligomer, and fibril Aβ concentrations [2]. A recent study was conducted to analyze the conformational

differences in Aβ from two different forms of GO [19]. Yet, another study also found that GO "maximally" expelled Aβ in mice and helped to improve fear memory in mice. This study established the effectiveness of GO as a treatment for Aβ-related diseases, such as AD [20]. Additionally, studies have found GO to be an acceptably biocompatible substance that can be used as a treatment in the future [17]. Alternative methods for treatment of AD are currently being studied. However, many treatments focus on tau inhibition as opposed to Aβ aggregation. The only treatments that are currently being used on patients focus on symptom treatments in lieu of treating the causes of AD [21]. These treatments include the use of three acetylcholinesterase enzyme inhibitors—donepezil, galantamine, and rivastigmine—and one N-methyl-D—aspartate receptor antagonist—memantine. Thus, combining the information from these different sources on Aβ towards AD, it can be ascertained that the focus on the biophysical interactions at a molecular level and on the use of 12 Aβ monomers that represent the ideal for the formation of a fibril, is clearly lacking.

The possibility of utilizing GO as a destabilizing agent against the accumulation of Aβ is the central theme of this study (Figure 1), which demonstrates how differently GO interacts with Aβ in various forms, such as monomers and fibrils, at an atomic level. Sections 3 and 4 report the effects of exposing GO to the early stages of Aβ aggregation in the form of an Aβ fibril and as an aggregation of individual Aβ monomers through various analytical strategies, including center of mass, Van der Waals interactions, RMSD (root mean square deviation), electrostatics, and salt bridge formation. The system is modeled as a fibril containing 12 Aβ monomers and a GO sheet within 7 Å of each other for simulations. These simulated trajectories are then compared to those of five Aβ monomers, both in the presence and absence (control) of a single layer of GO. The comparison of these simulations helped us to gain insights into the effects of GO on different numbers of Aβ monomers as well as how Aβ monomers interact amongst each other in the absence of GO.

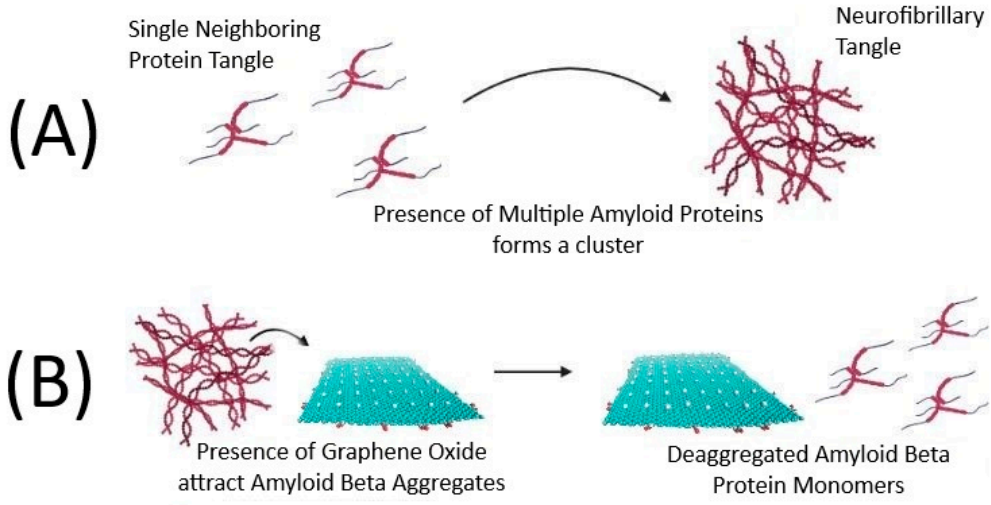

Figure 1. *Cont.*

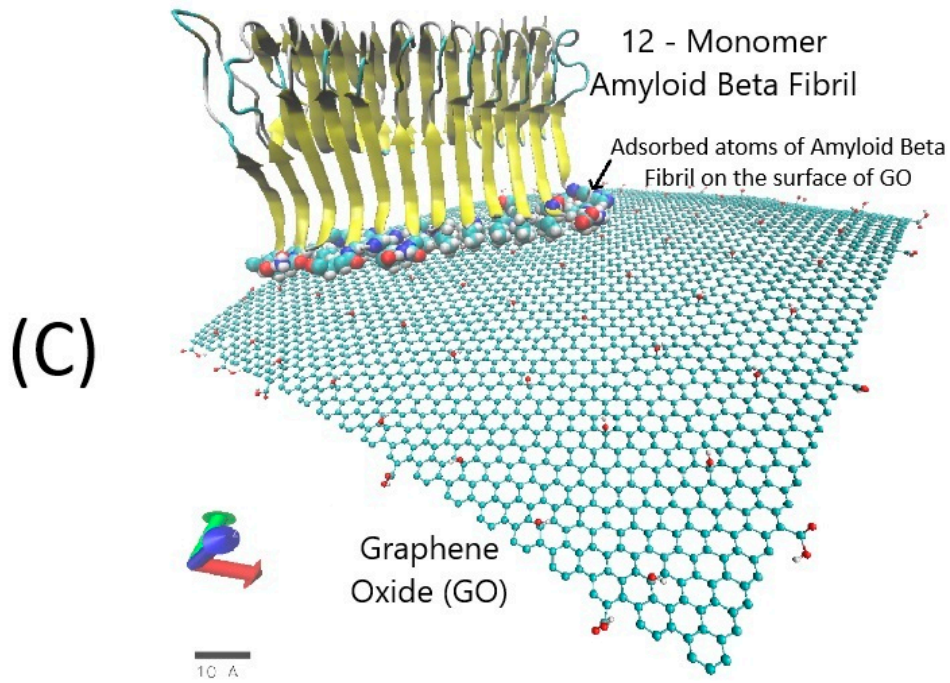

Figure 1. Role of GO in disentangling the neurofibrillary tangles. (**A**) Progression from a single Aβ monomer as a protein tangle to the formation of neurofibrillary tangle clusters; (**B**) GO attracts the Aβ tangles and disintegrates the neurofibrillary tangles; and (**C**) adsorption of the 12-monomer Aβ fibril onto the surface of GO showing the adsorbed atoms of Aβ.

2. Materials and Methods

This study was conducted utilizing the molecular graphics program, Visual Molecular Dynamics (VMD), version 1.9.3 [22] for modeling the molecular systems [22] containing GO and Aβ and analyzing the simulated trajectories. A molecular simulation program, Nanoscale Molecular Dynamics (NAMD), was used in conjunction with VMD for simulations [23]. The crystallographic information for the Aβ monomer (PDB ID: 1IYT) was acquired from the protein database (rcsb.org) consisting of the atomic coordinates. The Aβ fibril consisting of 12 monomers was modeled through VMD using the Aβ monomer acquired from the protein data bank. The structural file for GO was created using a molefacture plugin in VMD from the graphene sheet generated using an inbuilt graphene sheet builder plugin, which was then used to create a GO flake (size 15.45 Å × 11.68 Å). The chemical structure of the flake used is $C_{10}O_1(OH)_1(COOH)_{0.5}$, also known as oxidized GO (OGO). The structures of these molecules are modeled based on the Chemistry at Harvard Macromolecular Machines (CHARMM) topology files. The Aβ monomers, either 5 or 12, based on the system containing monomers or fibril, were placed next to each other within 15 Å of the neighboring monomer, and a GO sheet was placed equidistant, within 15 Å of Aβ. Interactive forces between GO and Aβ monomers as well as 12-monomer fibril were set up and analyzed using VMD, and the simulations were carried out using NAMD. All-atom simulations containing the Aβ monomers within the three different systems, with and without GO, and a 12 Aβ fibril with GO for a time period of 100 ns and 200 ns were carried out using the CHARMM [24] force field and TIP3 [25] water model. Neutralizing salt concentration of NaCl for effective polarization of the water molecules was used in all simulations. Intel Core i9 cluster with a total of 36 cores, and NVIDIA GeForce RTX 2080 GPU, purchased from Puget Systems, Auburn, WA, United States, was used to perform all the simulations, which took ~272 h (~0.02 s/step) for the individual Aβ simulations without GO, ~389 h (~0.028 s/step) for individual Aβ simulations with GO, and ~446 h (~0.032 s/step) for simulations involving Aβ fibril and GO. It should be noted that these times are considering other simulations going on in parallel with the i9 cluster.

In each simulation, the temperature was maintained at 300 K by a Langevin thermostat and a pressure of 1 atm through a Nose–Hoover Langevin Piston barostat with a period of 100 ps and a decay rate of 50 ps, assuming the periodic boundary conditions. A 10,000-step energy minimization was performed first to reach a stable state. All atom simulations employed an integrated time step of 2 fs. A cut-off of 12 Å designated the short-range forces while long-range forces were calculated using the Particle Mesh Ewald (PME) algorithm. RMSD and NAMD energy extensions were used to determine the stability and the interaction energy between the Aβ in the form of individual monomers, as a fibril with GO, and with each other (control). The VMD Timeline tool was used to analyze the secondary structure of Aβ during the simulations. TCL scripting was utilized to evaluate the distance between the centers of masses between the individual molecules. TCL was also used to evaluate the optimum cut-off distance between GO and Aβ monomers both individually and in the form of a fibril to determine the minimum number of Aβ atoms needed to have the maximum energy of interaction to achieve a stable complex. The rest of the analysis involving salt bridges, hydrogen bonds, conformational energy, and nonbonding energy was carried out using the available VMD plugins. TCL scripting was also used for the determination of the number of interfacial water molecules, and number of atoms of Aβ within 5 Å of GO. All datasets were plotted using the cloud-based data analysis and graphing software, OriginPro.

3. Results

Based on the primary goal of this study to quantify the differences between the interactions of Aβ fibril with GO and that of individual Aβ monomers in the presence and absence of GO, a quantification of the simulated trajectories with and without GO was undertaken and categorized into stability-based and energetics-based analyses involving exhaustive data collection and interpretation. A salt bridge analysis quantified the number of formed, broken, or sustained salt bridges between individual residues (amino acids) to measure the stability of the respective Aβ monomers as well as the Aβ fibril as a whole. RMSD measured the average deviation of a molecule's displacement and graphically showed the stability (or instability) aspects of the influence of GO on Aβ. While RMSD related one molecule to another in terms of its stability, the distance between the center of mass (COM) analyzed the effect of a molecule's distance with respect to another molecule on adsorption, thereby providing a scale to compare the closeness of molecules from each other. Van der Waals nonbonding energies were analyzed to show how Aβ in the form of individual monomers and as a fibril interacted with GO, and the combined electrostatics provided an overview of GO–Aβ bonding vs. Aβ–Aβ bonding in case of individual monomers. Through these analyses, we can visually interpret the combined results as well as account for unusual spikes when Aβ, in the form of either a monomer or as a fibril, adsorbs onto GO. Furthermore, the stability analysis also involved the number of hydrogen bonds, Aβ secondary structure analysis, and the quantification of conformational energies. While all these analyses are considered more of a basic quantification of the nature and role of the interface between Aβ and GO, a more exhaustive analysis in the form of energetics involved the quantification of electrostatic interactions within the Aβ monomers as independent units and in the form of fibril. A nonbonding energy analysis in the form of Van der Waals energies, an optimal adsorption distance analysis, the role of water molecules at the interface of individual Aβ monomers and GO, and those between the Aβ fibril and GO further confirmed the stability of interface between GO and Aβ. Screenshots of the simulation trajectories for the individual Aβ monomer system in the presence and absence of GO, and those for the system involving Aβ fibril can be found in the Supplementary Figures S1 and S2. It can be seen from these screenshots that the Aβ protein has two distinct secondary structures, as an α helix in the monomeric form and β sheets in the fibril form. It can also be seen that in the monomer form, Aβ forms two separate clumps, which are referred to as clump 1 (involving the Aβ segments titled AP1, 2AP1, and 3AP1), and clump 2 (involving the Aβ segments titled 1AP1 and 4AP1). The models that were constructed for

the present study along with their co-ordinates (PDB files), atomic structures (PSF), and parameter and configuration files have also been made available in the form of datasets. More details are available in the Data Availability Statement.

3.1. Stability

3.1.1. Salt Bridge Formation

Table 1 shows three situations, the control simulation of 5-Aβ without GO, 5-Aβ with GO, and 12-Aβ fibril with GO (12-Aβ-GO). In the control simulation, eight salt bridges are formed and no salt bridges are broken. This is the most stable of the three simulations. When GO is introduced, less salt bridges are formed, and more salt bridges are broken. This shows a trend in the decreasing stability of Aβ interactions with the presence of GO. Specifically, the common salt bridges between the presence and absence of GO trajectories (boldface in Table 1) indicate that the salt bridge between the residues GLU3 (glutamic acid, ID 3) and ARG5 (arginine, ID 5) on chain 4 is broken in the presence of GO, whereas in the absence of GO, it was formed. Furthermore, during the simulation of 12 Aβ fibrils, there is only one salt bridge formed, and there is one broken. This lack of the salt bridge formation and the presence of broken salt bridges demonstrate a lack of stability in the systems. This lack of stability indicates that GO interferes with the stability of the system in that the monomers undergo conformational changes, thereby losing the salt bridges and unable to form more stable salt bridges. Also, ASP7 (aspartic acid, ID 7) with ARG5 (arginine, ID 5) on chain 4, and GLU3 (glutamic acid, ID 3) with ARG5 (arginine, ID 5) on chain 2 are sustained in the presence of GO, whereas without GO, these bridges were formed. Sustained salt bridges only appear for the 5-Aβ with GO simulation. This indicates that GO constricts the movement of Aβ via adsorption. New salt bridges cannot form, but existing salt bridges are sustained. This stabilizes Aβ onto the surface of GO. Individual plots for all the salt bridges for the 5-Aβ and the 12-monomer Aβ fibril systems can be found in the Supplementary Figures S3–S5.

Table 1. Quantification of salt bridges within Aβ monomers (5-Aβ) and Aβ fibril (12-Aβ) in the presence and absence of GO.

Salt Bridge	Formed	Broken	Sustained
12-Aβ-GO Simulation			
ASP23 Chain A and LYS28 Chain A	✓		
GLU11 Chain C and LYS16 Chain B		✓	
5-Aβ no GO Simulation			
ASP7 Chain 2 and LYS28 Chain 2	✓		
ASP7 Chain 4 and ARG5 Chain 4	✓		
GLU3 Chain 2 and ARG5 Chain 2	✓		
GLU3 Chain 4 and ARG5 Chain 4	✓		
GLU11 Chain 2 and LYS28 Chain 2	✓		
GLU11 Chain 4 and ARG5 Chain 4	✓		
GLU11 Chain A and ARG5 Chain 3	✓		
GLU22 Chain A and LYS16 Chain 3	✓		
5-Aβ-GO Simulation			
GLU22 Chain A and LYS16 Chain 3	✓		
GLU11 Chain 3 and ARG5 Chain 3	✓		
GLU3 Chain A and LYS16 Chain A	✓		
GLU3 Chain 4 and ARG5 Chain 4		✓	
ASP23 Chain 3 and LYS28 Chain A	✓		

Table 1. *Cont.*

Salt Bridge	Formed	Broken	Sustained
ASP7 Chain 4 and ARG5 Chain 4			✓
ASP1 Chain A and ARG5 Chain A	✓		
GLU3 Chain 2 and ARG5 Chain 2			✓

3.1.2. Root Mean Square Deviation (RMSD) and Center of Mass (COM) Analysis

To further establish the stability of Aβ on GO, an RMSD analysis involving individual Aβ monomers in the presence and absence of GO, and an Aβ fibril in the presence of GO was performed. Figure 2A shows that the RMSD trajectory of the 12-Aβ-GO system is stable in the beginning of the simulation and continuously increases following 100 ns. Looking at the RMSD of GO, especially after 140 ns, it is clear that GO did play a role in destabilizing the Aβ fibril. On the contrary, Figure 2B shows a relatively stable 5-Aβ-GO complex following a brief period of destabilization at 40 ns indicating that the individual Aβ monomers adsorbed onto the surface of GO had more favorable and stable interactions. The relative instability of the 5-Aβ system in the absence of GO is indicative of the ongoing conformational changes within the Aβ monomers to form a complex. This relative stability of the monomers compared to the instability of the fibril in the presence of GO shows that the introduction of GO to the Aβ systems has a potential to cause a destabilization effect within the Aβ fibrils. Another factor to quantify stability is to consider the distance between the centers of masses (COM) between the two interacting molecules. As can be seen from Figure 2C, the COM of the 12-Aβ-GO simulation is stable until around 150 ns when it destabilizes, and the disturbance moves the fibril as close as 20 Å with respect to the center of mass of GO. Looking next at Figure 2D, the 5-Aβ monomer system was analyzed. In the presence of GO, the COM increased from ~30 Å to 45 Å after 60 ns. Without GO, the COM rapidly decreased from ~90 Å to 15 Å in 60 ns. This decrease indicates that GO promotes the Aβ monomers to move apart from each other, resulting in an increased COM measurement.

This change also shows that the individual Aβ monomers have a tendency to clump together in the absence of GO, further supporting the idea that the introduction of GO into the Aβ system prevents the aggregation of Aβ. The RMSD of individual Aβ monomers in the presence and absence of GO are available in the Supplementary Figure S6. Furthermore, the COM analysis for the individual Aβ monomers in the absence of GO can be found in the Supplementary Figure S7. These data show that the five Aβ monomers formed two separate clumps with monomers AP1, 2AP1, and 3AP1, forming one clump (clump 1), and the monomers 1AP1 and 4AP1, forming a second clump (clump 2). This further confirms the visual analysis from the trajectory screenshots of Supplementary Figure S1.

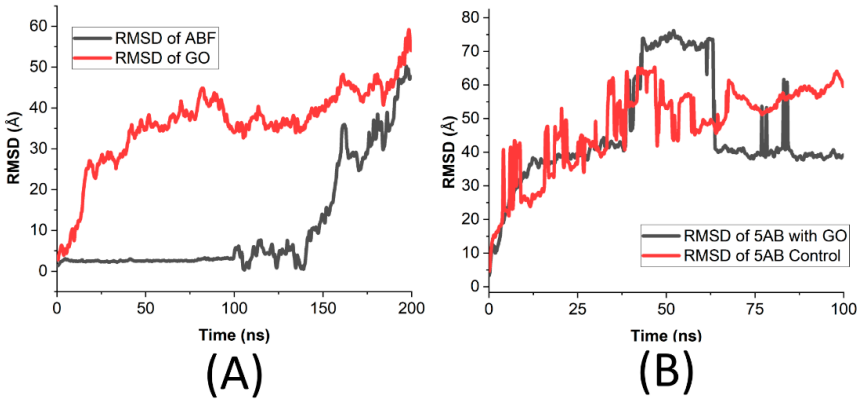

Figure 2. *Cont.*

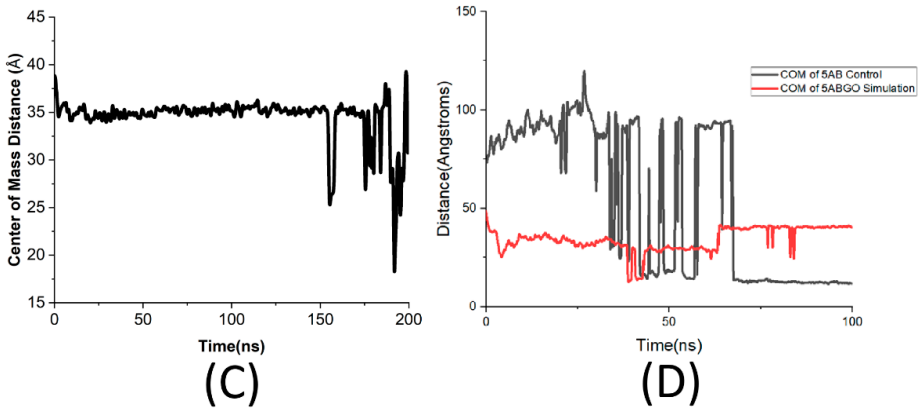

Figure 2. RMSD trajectories and COMs for individual Aβ monomers and 12-monomer Aβ fibril: (**A**) RMSD Trajectory of 12-Aβ-GO system; (**B**) average RMSD for the 5-Aβ system in the presence and absence of GO; (**C**) COM distance between GO and the Aβ fibril for the 12-Aβ-GO system; and (**D**) COM distance between the individual Aβ monomers in the presence and absence of GO for the 5-Aβ system.

3.1.3. Analysis of the Energetics

Different energies in the form of interaction energy and conformational energy play a vital role in understanding the interface between the two interacting molecules. To this end, a thorough analysis of the interaction energies (Van der Waals and electrostatics) and conformational energies (potential energies from the structure of bonds, angles, dihedrals, and improper) of the molecules was performed. Figure 3 shows these various nonbonding energies for both systems, 12-monomer Aβ fibril and 5-monomer Aβ systems. As shown in Figure 3A, the Van der Waals nonbonding energies between the fibril and GO started to stabilize as early as 25 ns to ~200 kCal/mol, whereas the electrostatic energy of the fibril fluctuated around ~1300 kCal/mol throughout the simulation. The conformational energy of the fibril structure was also constant around 7300 kCal/mol throughout the 200 ns simulation (Figure 3B). Compared to this constant conformational energy, the Van der Waals nonbonding energy between the individual 5 Aβ monomers and GO stabilized to ~250 kCal/mol starting ~60 ns. The overall electrostatic energy within the 5 Aβ monomers increased from ~1750 kCal/mol to ~3000 kCal/mol in the presence of GO and fluctuated around 2800 kCal/mol in the absence of GO. This fluctuation indicates that the presence of GO inhibited an increase in the electrostatic attraction within the Aβ monomers. This increase also supports the electrostatic energy data from the Aβ fibril, where it fluctuated around ~1300 kCal/mol (Figure 3A). Similar to the fibril system, the total conformational energy of the structure of 5-Aβ monomers was unaffected by the presence of GO and fluctuated around ~4175 kCal/mol (Figure 3D). The difference in the amount of the total conformational energies between the 5-Aβ monomeric system and the 12-Aβ fibril system is also indicative of the larger number of monomers present in the fibril system. However, interestingly, the increase in the conformational energy did not scale up accordingly. This also demonstrates the differences in the interactions between the monomers and their secondary structures when they are in the individual monomeric form, compared to the fibril form. The total conformational energy for the fibril system, as shown in Figure 3B, come from the individual potential energies emanating from the basic structure of the protein in the form of bonds, angles, dihedrals, and impropers. These individual potential energies were analyzed. The data can be found for the fibril system in Supplementary Figure S8. Further quantification of the interaction energies in the form of Van der Waals and conformational energies for the individual Aβ monomers in the presence and absence of GO can be found in the Supplementary Figure S9.

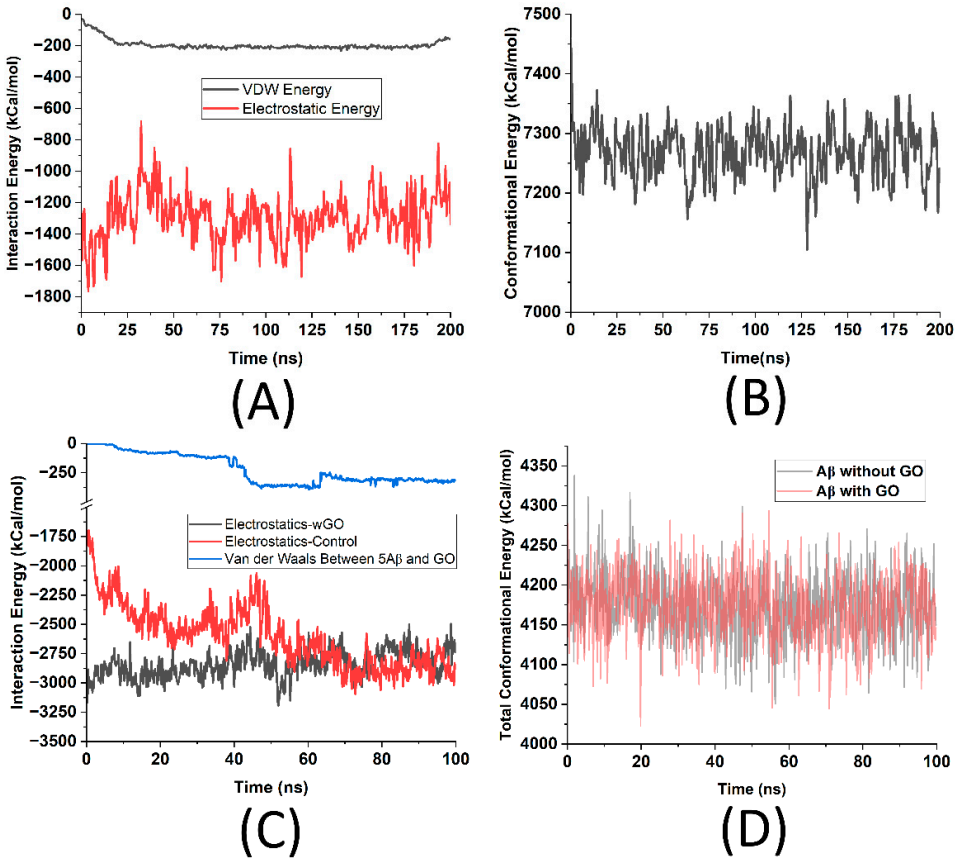

Figure 3. Interaction energies for 12-monomer Aβ fibril and individual 5-Aβ monomers: (**A**) Van der Waals energy between the Aβ fibril and GO and electrostatic energy within the Aβ fibril in the presence of GO; (**B**) total conformational energy of the Aβ fibril in the presence of GO; (**C**) electrostatic energy with 5-Aβ in the presence and absence of GO, and the total Van der Waals energy between 5-Aβ and GO; and (**D**) total conformational energy of 5-Aβ monomers in the presence and absence of GO. Note: wGO—with GO.

3.1.4. Hydrogen Bonds

The stability of the Aβ systems was also confirmed through the analysis of the hydrogen bonds within and between the Aβ monomers. As can be seen in Figure 4, the hydrogen bond analysis involved quantifying the number of hydrogen bonds. The hydrogen bonds were found to be much different between the fibril and monomeric forms of the Aβ. The fibril form had an average of ~115 hydrogen bonds overall throughout the simulation (Figure 4A), whereas the monomeric form of the Aβ showed an increasing trend in the absence of GO and a decreasing trend in the presence thereof (Figure 4B). This trend indicates that in the absence of GO, the Aβ tends to form more hydrogen bonds to create clump 1 and clump 2 that would eventually give rise to the formation of the fibril form of the Aβ. To further test this hypothesis, the number of hydrogen bonds within clump 1 and clump 2 in the absence of GO were analyzed, as shown in Figure 4C,D. This analysis gave the exact time period at which the hydrogen bonds were initiated between the monomers to facilitate the formation of the complexes. From Figure 4C, it is found that in the case of clump 1 between the segments AP1, 2AP1, and 3AP1, the hydrogen bonds increased in number and lifetime starting ~68 ns. Whereas in clump 2, between the segments 1AP1 and 4AP1, the hydrogen bonds started to form as early as 2 ns. The presence of short-lived hydrogen bonds between the segments, AP1 (clump 1) and 4AP1 (clump 2) in Figure 4D, also indicates that during the first 100 ns, the individual monomers of Aβ most likely prefer to form simple complexes of a doublet or a triplet, which would eventually form a more complex structure such as the well-known 12-monomer Aβ fibril. In summary, the data

seem to suggest that the presence of GO tends to decrease the number of hydrogen bond interactions between Aβ and hence prevents its aggregation. Individual plots of hydrogen bonds within the monomers of the 5Aβ system in the presence and absence of GO can be found in the Supplementary Figure S10.

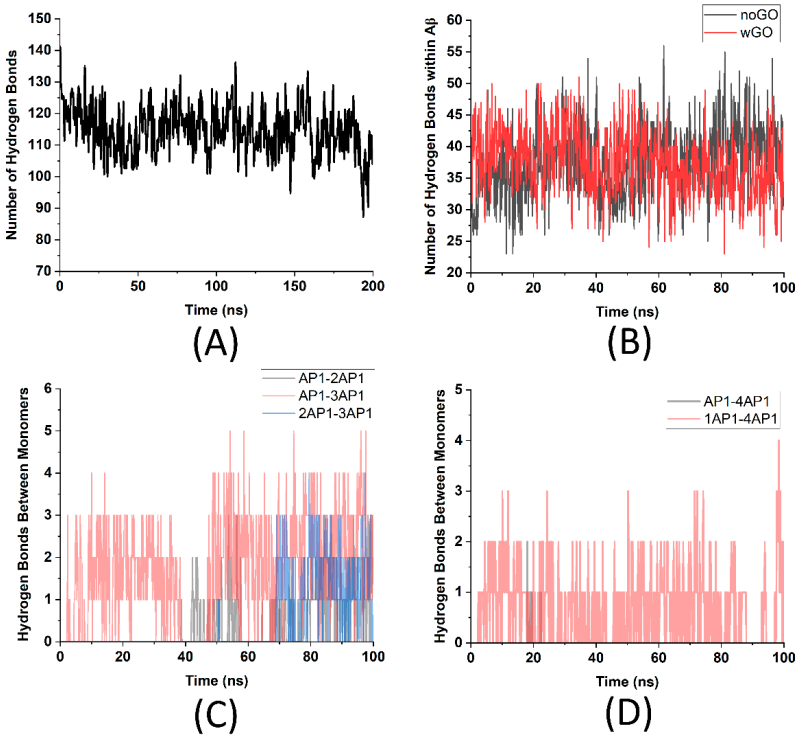

Figure 4. Analysis of hydrogen bonds to quantify stability. (**A**) hydrogen bonds within the Aβ fibril in the presence of GO; (**B**) hydrogen bonds within the 5 Aβ monomers in the presence and absence of GO; (**C**) hydrogen bonds between the Aβ monomers forming clump 1 involving the segments AP1, 2AP1, and 3AP1 in the absence of GO; and (**D**) hydrogen bonds between the Aβ monomers forming clump 2 involving the segments 1AP1 and 4AP1 in the absence of GO. Note: wGO—With GO; noGO—without GO.

A thorough analysis of the secondary structure of Aβ was undertaken, both as part of a fibril and as individual monomers in the presence and absence of GO. The color-coded plots for the secondary structures of individual monomers in the presence and absence of GO, and those for the fibril as a whole can be found in the Supplementary Figures S11–S15, for the 5 individual monomers and Supplementary Figure S16 for the Aβ fibril. It is found that in the presence of GO, the Aβ monomers tend to lose their secondary structure as indicated by the shrunken α helices for all the individual monomers (Supplementary Figures S11A–S15A) rendering them incapable to form clumps similar to the control simulations (Supplementary Figures S11B–S15B). It also suggests that the interaction of Aβ monomers with GO is much more favorable compared to interactions between individual monomers in the presence of GO. On similar lines, Supplementary Figure S16 shows how the presence of GO disrupted the secondary structure of four out of twelve monomers (shown within the black boxes on Supplementary Figure S16), indicating the physical disruption of the fibril.

3.2. Optimal Adsorption Distance and Role of Water Molecules

To further analyze the interface between Aβ and GO, the optimal adsorption distance of the Aβ atoms from the surface of GO was quantified. This analysis was performed for both the fibril system and the monomeric 5-Aβ system. A comparison was then made on the optimal adsorption distances based on the number of atoms as a function of distance

from the surface of GO and the interaction energy as a function of the distance from the surface of GO. Figure 5 compares these data between the fibril and 5-Aβ systems. As can be seen in Figure 5A,B, the analysis with and without hydrogen atoms is quite similar. Between the two systems, the number of atoms of Aβ increases linearly, starting ~3 Å from the surface of GO. Hydrogen, being small and chemically reactive, tends to interact rather quickly so the nonbonding interactions and the stability of the interface is more appropriately analyzed by considering the heavy atoms including carbon, nitrogen, and oxygen that make up the protein backbone. Towards this end, this analysis involved quantifying the optimal adsorption distance based on the total number of interfacial atoms with and without hydrogen. Similarly the interaction energies between the atoms of Aβ and those of GO was also quantified as a function of distance, both with and without hydrogen. As can be seen from Figure 5C,D, for both the fibril and monomeric 5-Aβ systems, the interaction energy continued to increase and started to stabilize ~7 Å from the surface of GO. It was found that the difference with and without hydrogen is quite large in case of the monomeric 5-Aβ system (Figure 5D) compared to the fibril system (Figure 5C). This can be attributed to the fact that in the case of the monomeric 5-Aβ system, the hydrogen atoms of the individual monomers of Aβ, in the form of α-helices, influence the neighboring Aβ molecule to a lesser extent than the Aβ in the form of β-sheets in case of the more regularly arranged fibril system. Finally, Figure 5E,F shows the ratios of the number of atoms (Figure 5A,B) to the interaction energies (Figure 5C,D) to quantify the optimal adsorption distance from the surface of GO. The dip in the plots indicate the optimal distance of adsorption with respect to the maximum interaction energy that is governed by the minimum number of atoms at the interface. As can be seen from the plots in Figure 5E,F, these distances differ between the fibril system and the monomeric 5-Aβ system at ~3.5 Å to 3 Å, respectively. Furthermore, the optimal adsorption distance, including hydrogen, is the same as without hydrogen, in the 5-Aβ system (~3 Å), which is quite different from the fibril system (~4 Å). This distance also indicates that in case of the fibril system, the hydrogen atoms more intimately influence the way the atoms of the fibril (as part of the β-sheet) interact with GO compared to those in case of the monomeric 5-Aβ system (as α-helix).

Lastly, the quantification of the interface between the Aβ systems and GO was conducted through the interfacial water molecules and their hydrogen bonds. It is known that the interfacial water plays a vital role in facilitating the interactions between the two molecules. Figure 6 shows the results found from this analysis of the Aβ fibril system (Figure 6A,B) as compared to the monomeric 5-Aβ system (Figure 6C,D). Depicted in Figure 6A, the fibril system's number of water molecules stabilized ~25 ns until ~150 ns. After 150 ns, they tended to decrease as the fibril interacted more favorably with the GO. However, this is not true. In the 5-Aβ monomer system, the number of interfacial water molecules stabilized at ~50 ns. The interface was maintained for the rest of the simulation run, indicating the differences in the way that a fibril of Aβ and Aβ monomers interact with GO. The same trend with the interfacial water molecules can be seen with the hydrogen bonds of interfacial water molecules in Figure 6B,D. It was found that after stabilizing the hydrogen bonds of the interfacial water molecules at 150 ns, the interface underwent instability starting at ~175 ns. The number of interfacial hydrogen bonds started to rapidly decrease. The number of interfacial hydrogen bonds during the 5-Aβ-GO simulation, on the other hand, steadily increased in the beginning of the simulation and then stabilized around 50 ns. This shows that the system itself and the interactions began to stabilize. The difference between the simulations demonstrates the effects of having a fibril form versus the monomer form of the Aβ. As the fibril form began in a more stable state, the destabilization of the number of interfacial hydrogen bonds indicates that the interactions between the individual monomers present in the system began to lessen. This loss of interactions indicated that GO did cause a destabilization of the aggregation in Aβ fibrils. The fact that the 5-Aβ-GO simulation began to stabilize indicates that further interactions between the monomers in the presence of GO were not entertained. The presence of GO prevents further

interactions and aggregation of Aβ monomers. The loss of stability in the 12-Aβ-GO simulation shows that GO started to interfere with the aggregated Aβ fibril. Additional detailed data showing the number of interfacial water molecules and their hydrogen bonds within the two clusters designated clump 1 and clump 2, as well as those between individual monomers and GO, can be found in the Supplementary Figures S17 and S18.

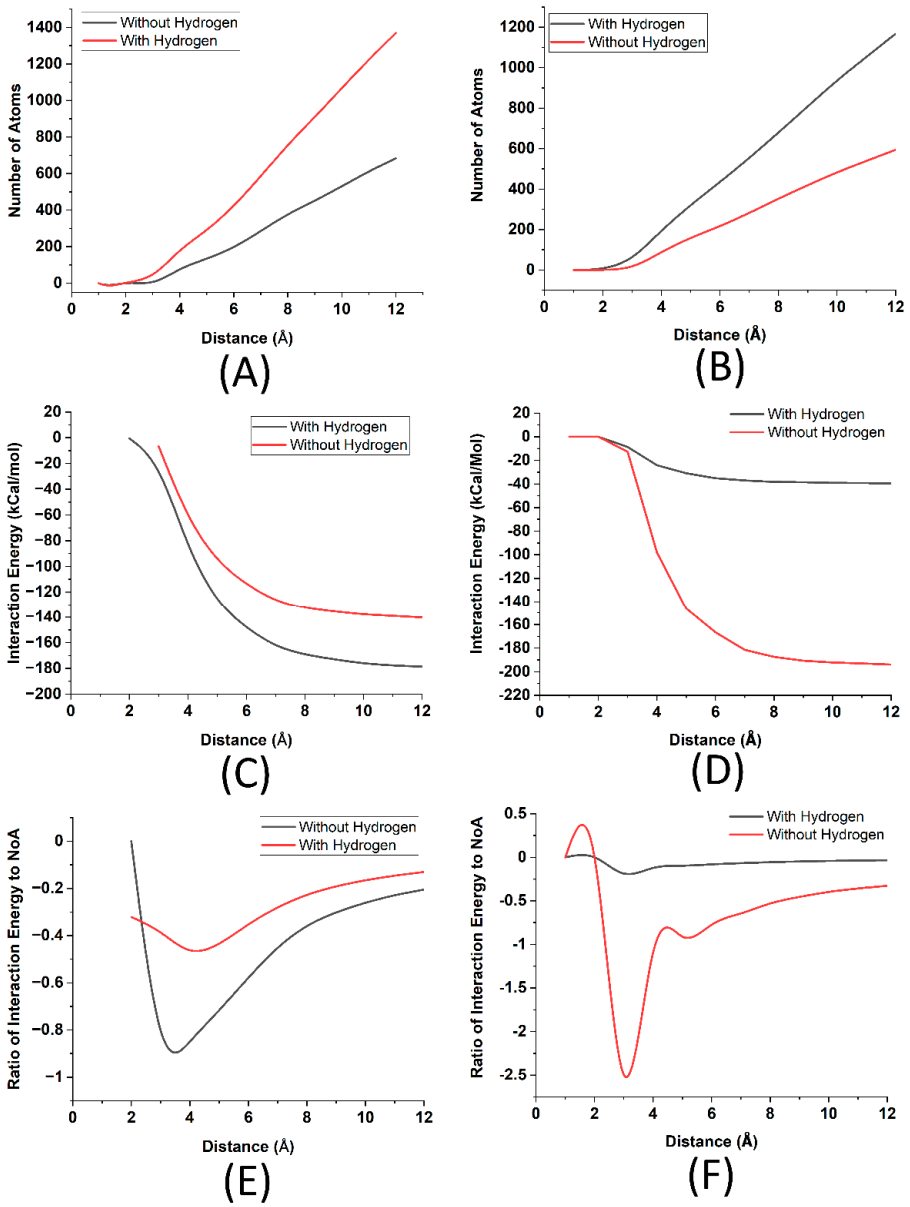

Figure 5. Optimal adsorption distance analysis based on the number of adsorbed atoms and interaction energy per adsorbed atom. (**A**) number of atoms with and without hydrogen as a function of the distance from the surface of GO for the Aβ fibril system; (**B**) number of atoms with and without hydrogen as a function of the distance from the surface of GO for the 5-Aβ system; (**C**) interaction energy of the adsorbed atoms as a function of the distance from the surface of GO for the Aβ fibril system; (**D**) interaction energy of the adsorbed atoms as a function of the distance from the surface of GO for the 5-Aβ system; (**E**) optimal adsorption distance as a function of the distance from the surface of GO for the Aβ fibril system; and (**F**) optimal adsorption distance as a function of the distance from the surface of GO for the 5-Aβ system.

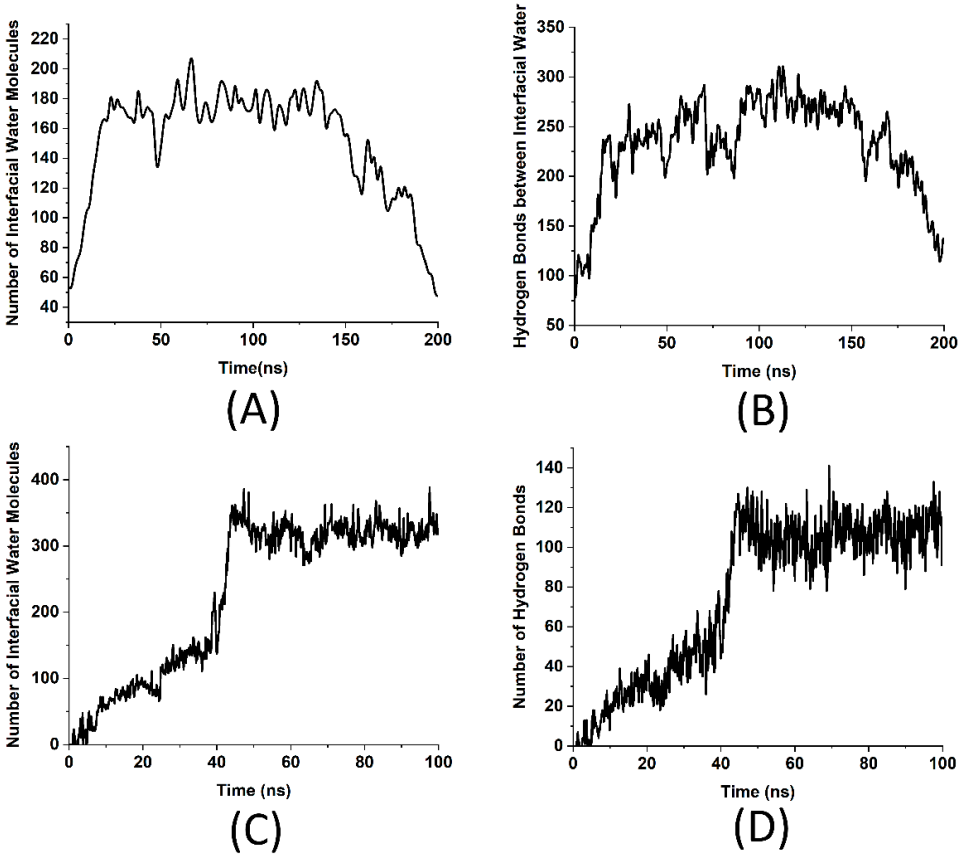

Figure 6. Quantification of the number of interfacial water molecules and their hydrogen bonds. (**A**) interfacial water molecules within 5 Å of GO and Aβ fibril; (**B**) hydrogen bonds of the interfacial water molecules during the interactions between Aβ fibril and GO; (**C**) total interfacial water molecules within 5 Å of GO and the monomeric 5-Aβ system; and (**D**) total number of hydrogen bonds of the interfacial water molecules during the interactions between individual Aβ monomers and GO.

4. Discussion

Based on the results and analysis of the simulated trajectories of Aβ fibril and monomeric Aβ with and without GO, it was found that GO has the potential to destabilize the aggregation of Aβ. This conclusion is supported by the stability analysis. That analysis showed that the presence of GO caused a reduction in salt bridge formations, significant RMSD deviations, an instability of fibril system COMs beyond 100 ns, and increased the COM of individual Aβ monomers from each other. Furthermore, more stable electrostatic interactions among the Aβ monomers, both in the monomeric and fibril form, in the presence of GO compared to the increased electrostatic interactions between the Aβ monomers in the absence of GO points to the mechanism by which Aβ monomers form larger assemblies. Interestingly, it was also found that in the presence of GO, the individual Aβ monomers did not interact through electrostatic energy. This finding suggests that this is the dominant form of interactions between the Aβ monomers in forming the fibril that would eventually give rise to the neurofibrillary tangles promoting AD. Finally, the stability was also analyzed through hydrogen bonds, where it was found that the number of hydrogen bonds decreased in the presence of GO for both within the monomeric structures and between the monomers. It is suggested that this may be the secondary mechanism in the formation of neurofibrillary tangles. There, the individual monomers form larger clumps through the hydrogen bonds, as seen in case of the control simulations of Aβ monomers having two distinct clumps (one with three monomers and another with two monomers). The presence of GO is found to target this hydrogen bonding as well where it inhibits

the formation of hydrogen bonds to prevent the aggregation of the Aβ monomers. This disintegration of Aβ monomers is also found to be affected indirectly by the changes in the secondary structure of the Aβ protein as evident from the secondary structure analysis. GO is found to significantly alter the secondary structure as the monomers and the fibril becomes adsorbed on its surface.

The conformational analysis further showed that the potential energies of the bonds, angles, dihedrals, and impropers of the Aβ, both in the fibril and in the monomeric form, stayed intact in the presence of GO. Furthermore, there are significant differences between the way the monomeric 5-Aβ interacted with GO compared to the 12-Aβ fibril. This demonstrates that the α helix of the Aβ in case of the monmeric system is affected much differently compared to the β-sheet structure of the Aβ fibril. The 12-Aβ fibril simulation with GO showed a more pronounced destabilization of the system, indicating that GO is effective in interfering with the aggregated Aβ in the form of a fibril. The secondary structure analysis of the monomeric Aβ also showed much disruption of the monomers in the presence of GO. However, it was found that the α helices in case of the Aβ monomers underwent a more significant shrinking compared to the β-sheets of a fibril system. An exhaustive analysis in the form of the optimal distance estimation of the adsorbed atoms of Aβ on the surface of GO and the role of interfacial water molecules and their hydrogen bonds are also found to be very different for the Aβ monomers compared to the fibril form. While the optimal distance of 3.5 Å was found for the fibril system for heavy atoms, it was found to be more than 4 Å for adsorbed atoms including hydrogen. Compared to this, the monomeric system had an optimal adsorption distance of 3 Å for heavy atoms and atoms including hydrogen. This suggests that in case of the fibril, hydrogen may be playing a more significant role in promoting the adsorption of the fibril to the surface of GO. Similarly, in case of the fibril system, the interfacial water molecules between the fibril and GO were found to decrease as stronger interactions between GO and the fibril ensued. This action resulted in reduced hydrogen bonds of the interfacial water molecules. However, in case of the adsorbed Aβ monomers on the surface of GO, the number of interfacial water molecules and their respective hydrogen bonds were found to be stable after the adsorption. This is yet another difference between the interactions of the fibril system and the monomeric system. These differences are influenced by their secondary structures. An individual analysis of the monomers and the clumps further support these interpretations.

In the future, it would be pertinent to extend simulations of Aβ-GO systems to show the prolonged effects of GO on the destabilization of the aggregation of Aβ. More specifically, extending the 12-Aβ-GO model by adding additional fibril and GO molecules would help with tracking the interactions in a more realistic manner. The extension of this system is necessary because the use of GO to treat AD in the future would entail long term usage and exposure of some form of GO to the brain. Further research could also study how these interactions are affected by the other chemical species present within the neural environment. Since the usage of GO to treat AD would interact with the chemicals in the brain, it is also important to ensure that GO is still effective at destabilizing the Aβ within the brain while also not having detrimental side effects on the neighboring healthy cells. While it is established that GO is a biocompatible substance, its in vivo effects are not yet fully understood, where several factors such as dose, administration route, and method of synthesis would play a crucial role on its effects on brain cells, which is yet to be extensively studied. In summary, this study has established that GO can be used to destabilize the Aβ accumulation found in patients with AD. The comparison between individual Aβ monomers and the Aβ fibril has potential to pave the way for future experiments involving in vitro and in vivo studies, with the latter having an effective shielding mechanism for GO.

5. Conclusions

Based on the results and analysis of this study, it is concluded that GO would be a useful molecule to address the disintegration and dispel the aggregation of Aβ. When considering salt bridges, hydrogen bonds, monomer interactions, and interfacial water

molecules, it is concluded that GO has a disrupting effect on the aggregation of Aβ and formation of Aβ fibrils. There is a notable difference between the effects of GO for the monomer form and fibril form of Aβ. However, the disintegrating effect of GO on the Aβ is similar for both forms of Aβ. This is evident from the stability and energetics analysis. Overall, the data show that GO holds a potential to disentangle the Aβ neurofibrillary tangles found in AD.

Supplementary Materials: The following supporting information can be downloaded at: https://www.mdpi.com/article/10.3390/c10040088/s1. Figure S1: trajectory screenshots for the 100 ns molecular simulations of the individual Aβ monomers: (A) 5 Aβ monomers after minimization and equilibration at 0 ns; (B) 5 Aβ monomers over the surface of graphene oxide (GO) at 50 ns; (C) 5 Aβ monomers over the surface of GO at 100 ns; (D) The 5 Aβ monomers in a control simulation in the absence of GO at 0 ns; (E) 5 Aβ monomers in the control simulation in the absence of GO at 50 ns; and (F) 5 Aβ monomers in the control simulation in the absence of GO at the end of a 100 ns simulation run. The Aβ monomers are represented with the New Cartoon representation in VMD, whereas GO and the sodium ions are represented with the CPK (Corey–Pauling–Koltun) model. Water molecules are not shown for clarity; Figure S2: trajectory screenshots for the 200 ns molecular simulation of the Aβ fibril in the presence of GO: (A) Aβ fibril on the verge of interacting with the GO surface after the minimization and equilibration runs and starting at 0 ns of the production run; (B) Aβ fibril adsorbed on the surface of GO at 100 ns in the simulation; (C) Aβ fibril firmly adsorbed on the surface of GO at the end of the simulation run at 200 ns. The Aβ fibril is represented with the New Cartoon representation in VMD, whereas GO and the sodium ions are represented with the CPK (Corey–Pauling–Koltun) model. Water molecules are not shown for clarity; Figure S3: plots showing individual salt bridges for the 5-Aβ system in the absence of GO (control simulation); Figure S4: plots showing individual salt bridges for the 5-Aβ system in the presence of GO; Figure S5: plots showing individual salt bridges for the 12-Aβ fibril system in the presence of GO; Figure S6: root mean square deviation (RMSD) of individual Aβ monomers within the 5-Aβ system, in the presence and absence of GO: (A) monomer segment AP1; (B) monomer segment 1AP1; (C) monomer segment 2AP1; (D) monomer segment 3AP1; (E) monomer segment 4AP1; Figure S7: plots showing distance between the center of mass of the individual monomers within the two clumps (clump 1 involving the segments AP1, 2AP1 and 3AP1, and clump 2 involving the two segments 1AP1 and 4AP1) in the absence of GO; Figure S8: conformational energy plots showing individual structural energies for the 12-Aβ fibril system in the presence of GO; Figure S9: interaction and conformational energies between and within the individual Aβ monomers of the 5-Aβ system: (A) interaction energy in the form of Van der Waals between the individual monomers within clump 1 and that between the monomers and GO; (B) interaction energy in the form of Van der Waals between the individual monomers within clump 2 and that between the monomers and GO; (C) conformational energies of the bonds, angles, dihedrals, and impropers of the individual monomers within the 5-Aβ system in the presence of GO; (D) conformational energies of the bonds, angles, dihedrals, and impropers of the individual monomers within the 5-Aβ system in the absence of GO; Figure S10: comparison of the number of hydrogen bonds within the individual Aβ monomers of the 5-Aβ system in the presence and absence of GO: (A) number of hydrogen bonds within the segment AP1 in the presence and absence of GO; (B) number of hydrogen bonds within the segment 1AP1 in the presence and absence of GO; (C) number of hydrogen bonds within the segment 2AP1 in the presence and absence of GO; (D) number of hydrogen bonds within the segment 3AP1 in the presence and absence of GO; (E) number of hydrogen bonds within the segment 4AP1 in the presence and absence of GO; Figure S11: secondary structure analysis of the segment AP1 in the presence (A) and absence (B) of GO; Figure S12: secondary structure analysis of the segment 1AP1 in the presence (A) and absence (B) of GO; Figure S13: secondary structure analysis of the segment 2AP1 in the presence (A) and absence (B) of GO; Figure S14: secondary structure analysis of the segment 3AP1 in the presence (A) and absence (B) of GO; Figure S15: secondary structure analysis of the segment 4AP1 in the presence (A) and absence (B) of GO; Figure S16: secondary structure analysis of the 12-monomer fibril; Figure S17: quantification of the number of interfacial water molecules and their hydrogen bonds within the two clumps: (A) the number of interfacial water molecules between the segments AP1, 2AP1 and 3AP1 of clump 1, and segments 1AP1 and 4AP1 of clump 2 in the presence of GO; (B) number of hydrogen bonds of the interfacial water molecules between the segments AP1, 2AP1

and 3AP1 of clump 1, and segments 1AP1 and 4AP1 of clump 2 in the presence of GO; (C) number of interfacial water molecules between the segments AP1, 2AP1 and 3AP1 of clump 1, and segments 1AP1 and 4AP1 of clump 2 in the absence of GO; (D) number of hydrogen bonds of the interfacial water molecules between the segments AP1, 2AP1 and 3AP1 of clump 1, and segments 1AP1 and 4AP1 of clump 2 in the absence of GO; Figure S18: quantification of the number of interfacial water molecules and their hydrogen bonds between the individual Aβ monomers and GO: (A) number of interfacial water molecules and their respective hydrogen bonds between segment AP1 and GO; (B) number of interfacial water molecules and their respective hydrogen bonds between segment 1AP1 and GO; (C) number of interfacial water molecules and their respective hydrogen bonds between segment 2AP1 and GO; (D) number of interfacial water molecules and their respective hydrogen bonds between segment 3AP1 and GO; (E) number of interfacial water molecules and their respective hydrogen bonds between segment 4AP1 and GO.

Author Contributions: Conceptualization, I.M.; methodology, I.W. and I.M.; software, I.W. and B.D.; validation, B.D. and I.M.; formal analysis, B.D. and I.W.; investigation, B.D., I.W. and I.M.; resources, I.M.; data curation, B.D. and I.M.; writing—original draft preparation, B.D. and I.W.; writing—review and editing, I.M.; supervision, I.M.; project administration, I.M. All authors have read and agreed to the published version of the manuscript.

Funding: This research received no external funding.

Data Availability Statement: The Modeling and Simulation software used in this study, VMD (Visual Molecular Dynamics) and NAMD (Nanoscale Molecular Dynamics), is freely available from the Theoretical and Computational Biophysics group at the NIH Center for Macromolecular Modeling and Bioinformatics at the University of Illinois at Urbana-Champaign, http://www.ks.uiuc.edu/Research/vmd/ (accessed on 1 September 2021). The atomic coordinate (protein data bank, PDB) file for the Aβ monomer, 1IYT, was obtained from the database located at the Research Collaboratory for Structural Bioinformatics (RCSB), www.rcsb.org (accessed on 1 September 2021). VMD was used to create the fibril structure combining the 12 monomers of Aβ protein by editing the PDB file, and the Nanotube builder plugin was used to create the GO molecule. To create the protein structure files (PSF) and to carry out all-atom simulations, the necessary topology and force field parameter files were obtained from the Chemistry at Harvard Macromolecular Mechanics (CHARMM) database located at the MacKerell Lab at the University of Maryland, School of Pharmacy, http://mackerell.umaryland.edu/charmm_ff.shtml (accessed on 30 September 2021). The models for the three systems, the Aβ fibril with GO, the 5 monomers of Aβ acting as a control, and the combined 5 Aβ and GO system along with the parameter and configuration files are also available as part of the Supporting Information.

Acknowledgments: The authors thank Fairfield University for providing the computational resources to carry out the simulations and analyze the simulated trajectories.

Conflicts of Interest: The authors declare no conflicts of interest.

References

1. Matthews, K.A.; Xu, W.; Gaglioti, A.H.; Holt, J.B.; Croft, J.B.; Mack, D.; McGuire, L.C. Racial and ethnic estimates of Alzheimer's disease and related dementias in the United States (2015–2060) in adults aged ≥ 65 years. *Alzheimer's Dement.* **2018**, *15*, 17–24. [CrossRef]
2. Chen, G.F.; Xu, T.H.; Yan, Y.; Zhou, Y.R.; Jiang, Y.; Melcher, K.; Xu, H.E. Amyloid beta: Structure, biology and structure-based therapeutic development. *Acta Pharmacol. Sin.* **2017**, *38*, 1205–1235. [CrossRef] [PubMed]
3. Goedert, M. Oskar Fisher and the study of dementia. *Brain* **2000**, *132*, 1102–1111. [CrossRef]
4. Glenner, G.G.; Wong, C.W. Alzheimer's disease and down's syndrome: Sharing of a unique cerebrovascular amyloid fibril protein. *Biochem Biophys. Res. Commun.* **1984**, *122*, 1131–1135. [CrossRef] [PubMed]
5. Masters, C.L.; Beyreuther, K. Amyloid Nomenclature Committee. *Amyloid* **1999**, *6*, 151–152. [CrossRef] [PubMed]
6. Coronel, R.; Bernabeu-Zornoza, A.; Palmer, C.; Muñiz-Moreno, M.; Zambrano, A.; Cano, E.; Liste, I. Role of Amyloid Precursor Protein (APP) and Its Derivatives in the Biology and Cell Fate Specification of Neural Stem Cells. *Mol. Neurobiol.* **2018**, *55*, 7107–7117. [CrossRef]
7. News Center. Scientists Reveal How Beta-Amyloid May Cause Alzheimer's. Available online: https://med.stanford.edu/news/all-news/2013/09/scientists-reveal-how-beta-amyloid-may-cause-alzheimers.html (accessed on 18 November 2020).
8. O'Brien, R.; Wong, P. Amyloid Precursor Protein Processing and Alzheimer's Disease. 2011. Available online: https://www.ncbi.nlm.nih.gov/pmc/articles/PMC3174086/ (accessed on 18 November 2020).

9. Smith, L.M.; Strittmatter, S.M. Binding Sites for Amyloid-β Oligomers and Synaptic Toxicity. *Cold Spring Harb. Perspect. Med.* **2016**, *7*, a024075. [CrossRef]
10. Jeong, D.; Kim, J.; Chae, M.S.; Lee, W.; Yang, S.H.; Kim, Y.; Kim, S.M.; Lee, J.S.; Lee, J.H.; Choi, J.; et al. Multifunctionalized Reduced Graphene Oxide Biosensors for Simultaneous Monitoring of Structural Changes in Amyloid-β 40. *Sensors* **2018**, *18*, 1738. [CrossRef] [PubMed] [PubMed Central]
11. Morley, J.E.; Farr, S.A. The role of amyloid-beta in the regulation of memory. *Biochem. Pharmacol.* **2014**, *88*, 479–485. [CrossRef]
12. Kahler, A.; Sticht, H.; Horn, A.H.C. Conformational Stability of Fibrillar Amyloid-Beta Oligomers via Protofilament Pair Formation—A Systematic Computational Study. *PLoS ONE* **2013**, *8*, e70521. [CrossRef]
13. Alzheimer's Association. 2020 Alzheimer's disease facts and figures. *Alzheimer's Dement.* **2020**, *16*, 391–460. [CrossRef] [PubMed]
14. Bhandari, W. Insight into Alzheimer's Early Stages Provides Clues to Treatment Strategies. 26 March 2020. Available online: https://medicine.wustl.edu/news/insight-into-alzheimers-early-stages-provides-clues-to-treatment-strategies/ (accessed on 18 November 2020).
15. Amyloid Plaques and Neurofibrillary Tangles. 13 March 2020. Available online: https://www.brightfocus.org/alzheimers-disease/infographic/amyloid-plaques-and-neurofibrillary-tangles (accessed on 18 November 2020).
16. Chae, M.S.; Kim, J.; Jeong, D.; Kim, Y.; Roh, J.H.; Lee, S.M.; Heo, Y.; Kang, J.Y.; Lee, J.H.; Yoon, D.S.; et al. Enhancing surface functionality of reduced graphene oxide biosensors by oxygen plasma treatment for Alzheimer's disease diagnosis. *Biosens Bioelectron.* **2017**, *92*, 610–617. [CrossRef] [PubMed]
17. Mahmoudi, M.; Akhavan, O.; Ghavami, M.; Rezaee, F.; Ghiasi, S.M.A. Graphene Oxide Strongy Inhibits Amyloid Beta Fibrillation. *Nanoscale* **2012**, *4*, 7322–7325. [CrossRef] [PubMed]
18. Li, M.; Yang, X.; Ren, J.; Qu, K.; Qu, X. Using graphene oxide high near-infrared absorbance for photothermal treatment of Alzheimer's disease. *Adv. Mater.* **2012**, *24*, 1722–1728. [CrossRef] [PubMed]
19. Baweja, L.; Balamurugan, K.; Subramanian, V.; Dhawan, A. Effect of graphene oxide on the conformational transitions of amyloid beta peptide: A molecular dynamics simulation study. *J. Mol. Graph. Model.* **2015**, *61*, 175–185. [CrossRef]
20. Zhang, J.; Zhu, S.; Jin, P.; Huang, Y.; Dai, Q.; Zhu, Q.; Wei, P.; Yang, Z.; Zhang, L.; Liu, H.; et al. Graphene oxide improves postoperative cognitive dysfunction by maximally alleviating amyloid beta burden in mice. *Theranostics* **2020**, *10*, 11908–11920. [CrossRef] [PubMed] [PubMed Central]
21. Vaz, M.; Silvestre, S. Alzheimers Disease: Recent Treatment Strategies. *Eur. J. Pharmacol.* **2020**, *887*, 173544. [CrossRef]
22. Humphrey, W.; Dalke, A.; Schulten, K. VMD: Visual molecular dynamics. *J. Mol. Graph.* **1996**, *14*, 33–38. [CrossRef]
23. Phillips, J.C.; Braun, R.; Wang, W.; Gumbart, J.; Tajkhorshid, E.; Villa, E.; Chipot, C.; Skeel, R.D.; Kalé, L.; Schulten, K. Scalable molecular dynamics with NAMD. *J. Comput. Chem.* **2005**, *26*, 1781–1802. [CrossRef]
24. MacKerell, A.D., Jr.; Bashford, D.; Bellott, M.; Dunbrack, R.L., Jr.; Evanseck, J.D.; Field, M.J.; Fischer, S.; Gao, J.; Guo, H.; Ha, S. All-Atom Empirical Potential for Molecular Modeling and Dynamics Studies of Proteins. *J. Phys. Chem. B* **1998**, *102*, 3586–3616. [CrossRef]
25. Jorgensen, W.L.; Chandrasekhar, J.; Madura, J.D.; Impey, R.W.; Klein, M.L. Comparison of simple potential functions for simulating liquid water. *J. Chem. Phys.* **1983**, *79*, 926–935. [CrossRef]